International Journal of Multiphase Flow 73 (2015) 34–42

Contents lists available at ScienceDirect

International Journal of Multiphase Flow

journal homepage: www.elsevier.com/locate/ijmulflow

Steady-state two-phase relative permeability functions of porous media: A revisit

C.D. Tsakiroglou [a,*], C.A. Aggelopoulos [a], K. Terzi [a], D.G. Avraam [b], M.S. Valavanides [c]

[a] Foundation for Research and Technology Hellas – Institute of Chemical Engineering Sciences, Stadiou Str., Platani, P.O. Box 1414, 26504 Patras, Greece
[b] Region of Central Macedonia, Regional Unity of Imathia, Department of Environment and Hydroeconomy, Mitropoleos 44, 59100 Veroia, Greece
[c] Technological Educational Institute of Athens, Department of Civil Engineering, Hydraulics Laboratory, Ag. Spyridonos, 12210 Aigaleo, Attika, Greece

ARTICLE INFO

Article history:
Received 4 August 2014
Received in revised form 27 February 2015
Accepted 4 March 2015
Available online 14 March 2015

Keywords:
Two-phase flow
Porous media
Relative permeability
Steady-state
Ganglion dynamics
Connected pathway flow
Electrical resistivity
Capillary number
Viscosity ratio

ABSTRACT

Steady-state two-phase flow experiments are performed on a sand column equipped with two differential pressure transducers and six ring electrodes to measure the pressure drop across each phase, and electrical resistance across five successive column segments, respectively. The electrical resistivity index measured across various segments of the soil column is converted to water saturation by using the Archie equation. The results are analyzed by considering the water saturation and oil/water relative permeability as power functions of water and oil capillary numbers which are employed as independent variables. Results from earlier visualization studies on a glass-etched pore network are also analyzed by a similar manner to quantify the dependence of oil and water relative permeability on capillary numbers, and correlate the estimated parameters of power functions with the viscosity ratio. The new explicit relationships of relative permeabilities and water saturation with oil and water capillary numbers set the bases for a new conceptualization of the two-phase flow at reservoir-scale where the mobility of the fluids is decoupled from saturation and become non-linear functions of the local flow rates. The variation of the relative permeability exponents with the pore system dimensionality agrees qualitatively with the scaling behavior predicted by the gradient percolation approach.

Introduction

Two-phase flow of immiscible fluids in porous media has attracted the attention of many research groups during the last 30 years (Payatakes, 1982; Lenormand et al., 1983; Dias and Payatakes, 1986a,b; Lenormand et al., 1988; Blunt and King, 1991; Vizika et al., 1994; Avraam and Payatakes, 1995a,b; Aker et al., 1998; Xu et al., 1998; Knudsen and Hansen, 2002; Tsakiroglou et al., 2003; Valvatne and Blunt, 2004; Li et al., 2005; Theodoropoulou et al., 2005; Joekar-Niasar et al., 2008; Aggelopoulos and Tsakiroglou, 2008; Tallakstad et al., 2009a; Raoof and Hassanizadeh, 2012). There is a broad variety of relevant application areas such as the enhanced oil recovery (Lackner and Torsaeter, 2006), the CO_2 storage in deep saline aquifers and depleted oil reservoirs (Berg and Ott, 2012), the soil contamination and reconstitution (Gao et al., 2013), the performance of proton exchange membranes in fuel cells (Wang et al., 2010). Sophisticated experimental setups have been developed to measure the steady-state relative permeability curves of porous media (Bentsen and Manai, 1991; Ayub and Bentsen, 2001), and analyze the interfacial viscous coupling effects (Ayub and Bentsen, 2004).

The steady-state two-phase flow is established by injecting two fluids through a porous medium at fixed flow rates, and has extensively be analyzed, primarily by computer simulations at pore- and network-scale (Constantinides and Payatakes, 1996; Valavanides et al., 1998; Hashemi et al., 1999; Ramstad and Hansen, 2006; Huang and Lu, 2009; Ramstad et al., 2012; Sinha and Hansen, 2012; Yiotis et al,. 2013), and secondarily by systematic experimental approaches in model porous media (Avraam et al., 1994; Avraam and Payatakes, 1995a, 1999; Tsakiroglou et al., 2007; Gutierez et al., 2008; Tallakstad et al., 2009a, 2009b; Erpelding et al., 2013). One of the main conclusions is that the wetting fluid (water) retains its connectivity along its flow path while the non-wetting fluid (oil) may move either as a connected pathway or as a population of disconnected ganglia which undergo dynamic breakup and coalescence (Avraam and Payatakes, 1995a; Constantinides and Payatakes, 1996; Valavanides et al., 1998; Tallakstad et al., 2009a, 2009b; Yiotis et al., 2013).

Numerous models and theoretical simulators have been developed to interpret the dependence of the two- and three-phase flow coefficients of porous media on the fractional/mixed wettability

* Corresponding author. Tel.: +30 2610965212; fax: +30 2610965223.
E-mail address: ctsakir@iceht.forth.gr (C.D. Tsakiroglou).

http://dx.doi.org/10.1016/j.ijmultiphaseflow.2015.03.001
0301-9322/

(Bradford et al., 1997; Tsakiroglou and Fleury, 1999; Jackson et al., 2003; Gladkikh and Bryant, 2006; Kuttanikkad et al., 2011; Tsakiroglou, 2014). Under mixed-wet conditions, that characterize the majority of natural porous media (e.g. rocks, soils), both fluids may contact the solid surfaces, the steady-state two-phase flow regimes are expected to become more complicated and the steady-state oil and water relative permeability are expected to change drastically (Landry et al., 2014). Therefore, any results obtained with experiments conducted on homogeneous-wet porous media cannot be extrapolated explicitly to mixed-wet porous media. Instead, a systematic analysis of the effects of heterogeneous wettability on the steady-state two-phase flow regimes and its implications to relative permeability functions is required.

Both the two-phase flow regimes and relative permeability functions of the two fluids depend strongly on a variety of key parameters such as the capillary number, flow rate ratio, viscosity ratio, wettability, and Bond number (Avraam and Payatakes, 1995a, 1999; Gutierez et al., 2008; Tallakstad et al., 2009b). In order to interpret quantitatively such a behavior, pore-network simulators (Constantinides and Payatakes, 1996; Ramstad and Hansen, 2006; Sinha and Hansen, 2012), Lattice-Boltzman approaches (Huang and Lu, 2009; Ramstad et al., 2012; Yiotis et al., 2013), and sophisticated mesoscopic approaches (Valavanides and Payatakes, 2001) have been developed. Nevertheless, albeit the aforementioned attempts revealed the multi-correlated character of the process, when simulating the two-phase flow at field-scale, mainly on industrial scale applications, the relative permeability of wetting and non-wetting fluids are still regarded as power functions of the local saturation and their implicit dependence on other parameters, such as the local flow rates is ignored.

The scope of the present work is to re-examine the rate-dependent oil/water relative permeabilities for steady-state co-current two-phase flow in porous media, and produce explicit correlations of fluid relative permeability and saturation with the oil and water capillary numbers. Steady-state two-phase flow experiments are performed on a sand column equipped with two differential pressure transducers and six ring electrodes to measure the pressure drop across each phase, and electrical resistance across five successive column segments, respectively. The oil to water viscosity ratio is kept equal to one in order to focus exclusively on the effect of capillary numbers on relative permeabilities. The electrical resistance is converted to water saturation based on a calibrated Archie-type equation. The results are analyzed by considering the water saturation and oil/water relative permeability as power functions of water and oil capillary numbers. Results from earlier experimental studies on 2-D porous media (Avraam and Payatakes, 1995a) are also analyzed in a similar manner so that the sensitivity of the relative permeabilities to capillary numbers is quantified for 2-D porous media.

Methods and materials

Experimental procedure

Steady-state experiments of the simultaneous flow of oil and water were performed on a long horizontal PVC column ($D = 5$ cm, $L = 30$ cm) packed with a well-sorted sand ($k = 25$ D, $\varphi = 0.42$) and equipped with ring electrodes and a multi-point conductivity meter used to monitor the electrical conductance along the column (Fig. 1, Aggelopoulos and Tsakiroglou, 2008). All measuring devices were connected to a data acquisition card equipped in the host computer. The apparatus was placed inside a thermostatic incubator so that the temperature was kept constant and equal to 25 °C to avoid any disturbances of electrical conductance. Two metallic plates placed in the inlet and outlet of the column acted as end current electrodes whereas six (6) intermediate rings placed at equal distances along the column were used as voltage electrodes. To improve the electrical contact of the soil with the end electrodes, ensure the uniform distribution of the flow across the column inlet/outlet, and avoid the entrainment of soil grains, two stainless steel screens were inserted between the end electrodes and the soil. The multi-point conductivity meter allowed the simultaneous measurement of the electrical resistance across various segments of the column with respect to a reference electrode. More details concerning the determination of the electrical resistance over the successive segments of the column from measurements of the corresponding voltages are reported elsewhere (Aggelopoulos and Tsakiroglou, 2008). The pressure drop across each phase was measured with the aid of pressure transducers connected to the inlet tubes (Fig. 1). First, the sand column was evacuated and filled with brine (aqueous solution of NaCl at concentration $C_{NaCl} = 20$ g/L). Then, oil (mixture composed of 61% n-C_{10} and 39% n-C_{12}) was injected at a high flow rate ($q_o = 5$ ml/min) until attaining an irreducible wetting phase saturation. Afterwards, oil and brine (viscosity ratio, $\kappa = \mu_o/\mu_w = 1.0$), were co-injected at flow rates 5 ml/min and 0.5 ml/min, respectively, by using two high performance liquid chromatography (HPLC) pumps (Fig. 1). The viscosity ratio was kept equal to one to exclude its effect on relative permeabilities and saturation and isolate it from that of the capillary numbers. Steady-state conditions were established when the time-averaged oil and water injection pressures along with the time-averaged electrical conductance were stabilized. Then, the oil flow rate was kept constant and the water flow rate varied stepwise from 0.5 to 5.0 ml/min in successive bumps. At each step, the column-averaged steady-state relative permeability of oil $\langle k_{ro} \rangle$ and water $\langle k_{rw} \rangle$ phase were calculated by using the Darcy law and the measured time-averaged pressure drop across the oil and water phases, respectively

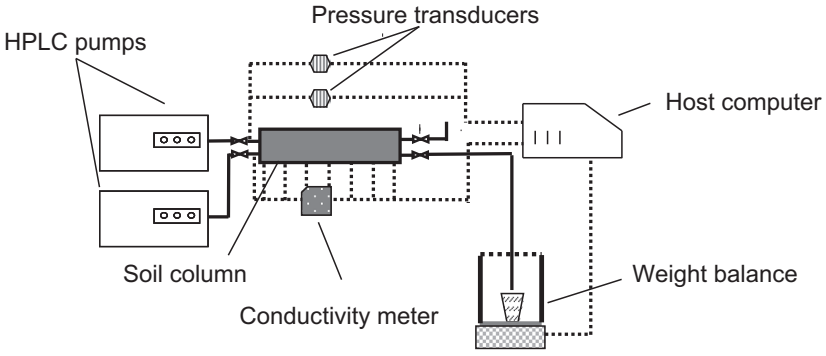

Fig. 1. Experimental setup of steady-state two-phase flow tests in soil columns.

$$\frac{q_w}{A} = \frac{k\langle k_{rw}\rangle}{\mu_w}\frac{\Delta P_w}{L} \tag{1a}$$

$$\frac{q_o}{A} = \frac{k\langle k_{ro}\rangle}{\mu_o}\frac{\Delta P_o}{L} \tag{1b}$$

At the end of each steady-state step, the effluent was weighted and the total water saturation of the soil column, $\langle S_w\rangle$, was estimated. The resistivity index, I_R, of a porous medium that is partially-saturated with an electrolyte solution is defined as the ratio of its electrical resistance to the electrical resistance that would be measured if the pore volume was fully-saturated by an electrolyte solution of equal concentration. The measured $I_R - \langle S_w\rangle$ data were fitted to an Archie power law of the form

$$I_R = \langle S_w\rangle^{-n} \tag{2}$$

so that the saturation exponent, n, was estimated. It was observed that the I_R values measured with the resistivity meter and the $\langle S_w\rangle$ values calculated from effluent weights could be fitted with a unique n value, so that any eventual changes of n with the flow rates were overlooked. The saturation exponent estimated from resistivity data across the entire sand column along with the values of resistivity index measured across each segment of the soil column, $(I_R)_{ij}$, were replaced in Eq. (2) to calculate the steady-state water saturation averaged over each segment of the column, $\langle S_w\rangle_{ij}$. The water flow rate was kept constant and the oil flow rate decreased to q_o = 1.0 ml/min. When steady-state conditions were established, the flow rate of oil was stabilized and the water flow rate started to decrease stepwise from 5.0 to 0.5 ml/min so that the steady-state oil and water relative permeability were determined at each step. The entire procedure was also repeated for oil flow rates q_o = 0.5 and 0.25 ml/min. In total, the oil and water relative permeability were determined for 16 steady-state steps each corresponding to a different pair of oil and water flow rates. Average values of water saturation were calculated for each intermediate segment of the column as well as for the entire column.

Relative permeabilities and numerical fitting

Visualization studies have revealed that the relative permeability functions are correlated strongly with the dominant steady-state two-phase flow regimes that are classified with respect to the distribution and mobility of non-wetting oleic phase (Avraam and Payatakes, 1995a, 1995b, 1999): (1) in the Connected Pathway Flow (CPF), the oil retains its hydraulic continuity across the porous medium, whereas the oil relative permeability is relatively high and does not change significantly with the flow rate of the wetting fluid; (2) in the Ganglion Dynamics (GD), the oil is disconnected into large ganglia (LGD), small ganglia (SGD), and drops of size less than that of a single pore (drop traffic flow, DTF), whereas the oil relative permeability is relatively low and is affected evidently by the water flow rates. The water saturation averaged over an area of the porous medium is decided by the pore space morphology, boundary conditions, water and oil flow rates, and some other properties (e.g. wettability, viscosity ratio) which are commonly kept constant during a steady-state experiment. Conventionally, the measured water and oil relative permeability, which express the hydraulic conductivity of each phase, are non-unique functions of saturation. For instance, identical water saturation accomplished by two different pairs of water and oil flow rates may correspond to two different values of water and oil relative permeability. Nevertheless, the water and oil relative permeability are commonly fitted with Corey type power functions of water saturation with parameters that change with fluid flow rates (Tsakiroglou et al., 2007).

To avoid the aforementioned inconsistency, a new formulation is introduced here, where both water saturation and relative permeability are regarded as dependent variables. For each step, the water saturation, $\langle S_w\rangle$, and steady-state oil, $\langle k_{ro}\rangle$, and water, $\langle k_{rw}\rangle$, relative permeability, all measured as average values over the entire soil column, can be regarded as functions of two independent variables: the water, Ca_w, and oil, Ca_o, capillary numbers defined by

$$Ca_w = \mu_w q_w (A\gamma_{ow}) \tag{3a}$$

$$Ca_o = \mu_o q_o (A\gamma_{ow}) \tag{3b}$$

where μ_i = viscosity of phase i (i = w,o), q_i = flow rate of phase i (i = w,o), γ_{ow} = interfacial tension, A = cross-sectional area of porous medium. The dependence of $\langle k_{rw}\rangle$, $\langle k_{ro}\rangle$, $\langle S_w\rangle$ on Ca_w, Ca_o, is described by power laws of the form

$$\langle k_{rw}\rangle = a_w Ca_w^{b_w} Ca_o^{b_o} \tag{4}$$

$$\langle k_{ro}\rangle = a_o Ca_w^{e_w} Ca_o^{e_o} \tag{5}$$

$$\langle S_w\rangle = a_s \mathrm{Ca}_w^{m_w} \mathrm{Ca}_o^{m_o} \tag{6}$$

The exponents (b_w, b_o, e_w, e_o, m_w, m_o), quantifying the rate-dependency of $\langle k_{rw}\rangle$, $\langle k_{ro}\rangle$, $\langle S_w\rangle$, are independent of the dominant flow regime, and are governed by a variety of "system parameters" (e.g. viscosity ratio, porous medium properties, wettability, dimensionality). Among other parameters (e.g. pore space morphology, permeability, etc.), the pre-exponential factors a_w, a_o, a_s depend on boundary conditions and may vary locally. At relatively very low Ca_w values and significant Ca_o values, the water saturation is low and the steady-state flow regime is dominated by CPF (Avraam and Payatakes, 1995). At progressively higher Ca_w values, the oil is disconnected into ganglia that move and undergo coalescence, break-up, fission, and entrapment. Under such conditions, no uninterrupting oil column connecting the inlet with the outlet of the porous medium can be sustained, and the steady-state flow regime is expected to be dominated by GD (Avraam and Payatakes, 1995a).

The data obtained from the experimental procedure described earlier were fitted using Eqs. (4)–(6) to estimate all unknown parameters with the aid of Athena Visual Studio (Stewart and Caracotsios, 2008). For the sake of completeness, the same equations were used to fit earlier datasets of steady-state two-phase flow experiments performed on a 2-D glass-etched pore network for two values of the capillary number, $\kappa = \mu_o\mu_w$ = 1.45, 3.35 (Avraam and Payatakes, 1995a).

Results and discussion

From the fitting of $I_R - \langle S_w\rangle$ datasets to Archie equation, Eq. (2), the saturation exponent n = 1.06 ± 0.0041 was obtained and used to convert the electrical resistivity to water saturation (Fig. 2). It is evident that the average water saturation over each of the five successive segments of the soil column, $\langle S_w\rangle_{ij}$ (ij = 12, 23, 34, 45, 56) varies sensibly (Fig. 2) and this might be attributed to the non-fully developed 1-D flow taking place near the column ends, in combination with capillary end effects (Aggelopoulos and Tsakiroglou, 2008). When both fluids are injected simultaneously, the irreducible water entrapped in the porous medium at the end of the displacement reconnects with the bulk phase and the water saturation increases rapidly in the first segments of the column (Fig. 2a). We can assume that the water saturation of each segment follows a power law with identical exponents, namely

$$\langle S_w\rangle_{ij} = (a_s)_{ij} \mathrm{Ca}_w^{m_w} \mathrm{Ca}_o^{m_o} \tag{7}$$

where the coefficients $(a_s)_{ij}$ are primarily governed by boundary conditions. The column-averaged coefficient, a_s, is expected to be equal to the arithmetic mean of the local coefficients, $(a_s)_{ij}$, namely

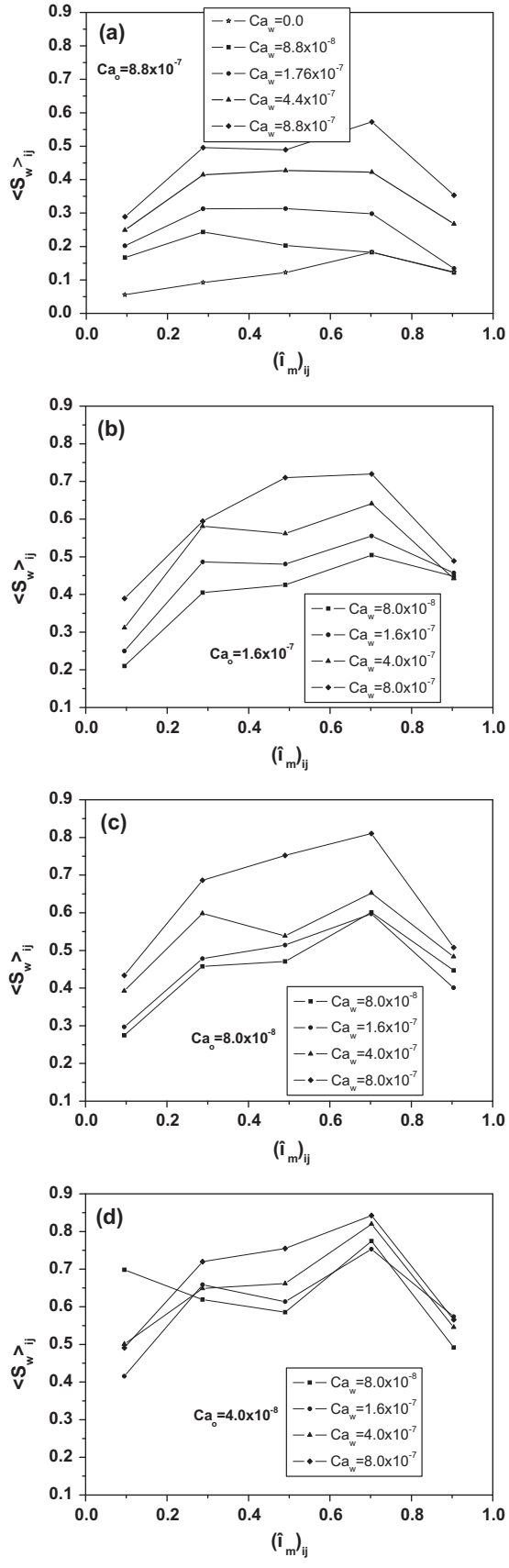

Fig. 2. Variation of the axial profile of water saturation with capillary numbers: (a) $Ca_o = 8.8 \times 10^{-7}$, (b) $Ca_o = 1.76 \times 10^{-7}$, (c) $Ca_o = 8.8 \times 10^{-8}$, (d) $Ca_o = 4.4 \times 10^{-8}$.

$$a_s = \sum_{ij} \xi_{ij} (a_s)_{ij} \tag{8}$$

The calculated column-averaged oil, $\langle k_{ro} \rangle$, and water, $\langle k_{rw} \rangle$, relative permeability along with the column-averaged water saturation, $\langle S_w \rangle$, are given as functions of the water and oil capillary numbers in Table 1.

The water saturation datasets (Fig. 2, Table 1) were simultaneously fitted to Eqs. (6) and (7) to estimate the parameters m_w, m_o, $(a_s)_{ij}$ ij = 12, 23, 34, 45, 56 and calculate a_s using Eq. (8). In addition, the datasets of the 2-D experiments (Avraam and Payatakes, 1995) were fitted to Eq. (6) to estimate the parameters m_w, m_o, a_s. The corresponding results are presented in Table 2. The wetting aqueous phase is continuous throughout a 2-D or 3-D porous medium and a similar behavior of water saturation as a function of the water capillary number is expected for 3-D and 2-D porous media (Table 2). On the other hand, in a 3-D pore system, connected pathways of the two fluids may co-exist over a broader range of Ca_w values leading to a stronger sensitivity of $\langle S_w \rangle$ to Ca_o and a lower value of exponent m_o (Table 2). In the 2-D pore network, the measurements are taken within a central area located far from the inlet and outlet ports where the flow is fully developed (Avraam and Payatakes, 1995a) and the boundary effects are eliminated so that the estimated parameter a_s is close to unity. In contrast, in the 3-D soil column, the boundary effects are evident particularly with reference to the end soil segments (Fig. 2), the water saturation is not uniform, and the estimated parameters a_s and $(a_s)_{ij}$ are relatively low (Table 2).

Table 1
Measured relative permeabilities and water saturation averaged over the soil column as functions of the water and oil capillary numbers.

Step	$\langle k_{rw} \rangle$	$\langle k_{ro} \rangle$	$\langle S_w \rangle$	Ca_w	Ca_o
0	0.0		0.1153	0.0	8.77752E−07
1	0.014559804	0.15827211	0.1836	8.77752E−08	8.77752E−07
1	0.026133285	0.14903862	0.2522	1.7555E−07	8.77752E−07
1	0.056067172	0.11377584	0.3561	4.38876E−07	8.77752E−07
1	0.093955146	0.10941324	0.44	8.77752E−07	8.77752E−07
2	0.142863652	0.03503166	0.5804	8.77752E−07	1.7555E−07
2	0.080650207	0.04061822	0.5075	4.38876E−07	1.7555E−07
2	0.032106138	0.03851323	0.4456	1.7555E−07	1.7555E−07
2	0.017238896	0.04492634	0.3986	8.77752E−08	1.7555E−07
3	0.022425678	0.03098493	0.4502	8.77752E−08	8.77752E−08
3	0.045518486	0.03169117	0.4574	1.7555E−07	8.77752E−08
3	0.102709684	0.02762538	0.533	4.38876E−07	8.77752E−08
3	0.185467685	0.02397212	0.6378	8.77752E−07	8.77752E−08
4	0.206780224	0.01374042	0.6747	8.77752E−07	4.38876E−08
4	0.110982598	0.01558945	0.6353	4.38876E−07	4.38876E−08
4	0.045726374	0.01554617	0.6028	1.7555E−07	4.38876E−08
4	0.021416156	0.01479582	0.6338	8.77752E−08	4.38876E−08

Table 2
Estimation of the parameters of water saturation relationship.

Parameter	3-D soil column	2-D glass-etched pore network (κ = 1.45)	2-D glass-etched pore network (κ = 3.35)
m_w	0.1321 ± 0.032	0.1320 ± 0.028	0.144 ± 0.0241
m_o	−0.2261 ± 0.030	−0.100 ± 0.0215	−0.1126 ± 0.0183
a_s	0.10 ± 0.068	0.8564 ± 0.23	0.8939 ± 0.0183
$(a_s)_{12}$	0.072 ± 0.049		
$(a_s)_{23}$	0.1069 ± 0.065		
$(a_s)_{34}$	0.1087 ± 0.073		
$(a_s)_{45}$	0.1255 ± 0.085		
$(a_s)_{56}$	0.0866 ± 0.059		

Table 3
Estimation of the parameters of oil relative permeability relationship.

Parameter	2-D glass-etched pore network (κ = 1.45)	2-D glass-etched pore network (κ = 3.35)	3-D soil column
a_o	24.17 ± 23.69	127.14 ± 116.0	241.5 ± 225.1
e_w	−0.197 ± 0.10	−0.0903 ± 0.094	−0.1667 ± 0.0393
e_o	0.6405 ± 0.121	0.639 ± 0.104	0.7202 ± 0.0507

Table 4
Estimation of the parameters of water relative permeability relationship.

Parameter	2-D glass-etched pore network (κ = 1.45)	2-D glass-etched pore network (κ = 3.35)	3-D soil column
a_w	29.14 ± 29.81	14.22 ± 24.7	629.01 ± 629.8
b_w	0.6458 ± 0.0936	0.583 ± 0.164	0.8845 ± 0.0606
b_o	−0.1781 ± 0.0519	−0.1872 ± 0.098	−0.255 ± 0.0307

Due to the boundary effects, the spatial distribution of fluids over the various soil column segments is reflected in corresponding relative permeability functions expressed by

$$\langle k_{rw}\rangle_{ij} = (a_w)_{ij} Ca_w^{b_w} Ca_o^{b_o} \tag{9}$$

$$\langle k_{ro}\rangle_{ij} = (a_o)_{ij} Ca_w^{e_w} Ca_o^{e_o} \tag{10}$$

where the values of the local coefficients, $(a_w)_{ij}$, $(a_o)_{ij}$, may change over the various segments, but the exponents b_w, b_o, e_w, e_o, m_w, m_o remain unaltered regardless of the dominant flow regime (as previously stated, they depend on *system* parameters). The relative permeability of each phase is proportional to its hydraulic conductivity and inversely proportional to its hydraulic resistance. The soil column can be regarded as resistors (segments) in series and therefore the column-averaged relative permeabilities are given by relationships of the form

$$\frac{1}{\langle k_{rw}\rangle} = \sum_{ij} \frac{\xi_{ij}}{\langle k_{rw}\rangle_{ij}} \qquad \frac{1}{\langle k_{rw}\rangle} = \sum_{ij} \frac{\xi_{ij}}{\langle k_{rw}\rangle_{ij}} \tag{11}$$

which are equivalently written as

$$\frac{1}{a_w} = \sum_{ij} \frac{\xi_{ij}}{(a_w)_{ij}} \qquad \frac{1}{a_o} = \sum_{ij} \frac{\xi_{ij}}{(a_o)_{ij}} \tag{12}$$

According to Eq. (12), the column-averaged relative permeabilities and coefficients a_w, a_o are the geometric means of the segment-averaged relative permeabilities and local coefficients, $(a_w)_{ij}$, $(a_o t)_{ij}$. The water and oil relative permeability datasets were fitted using

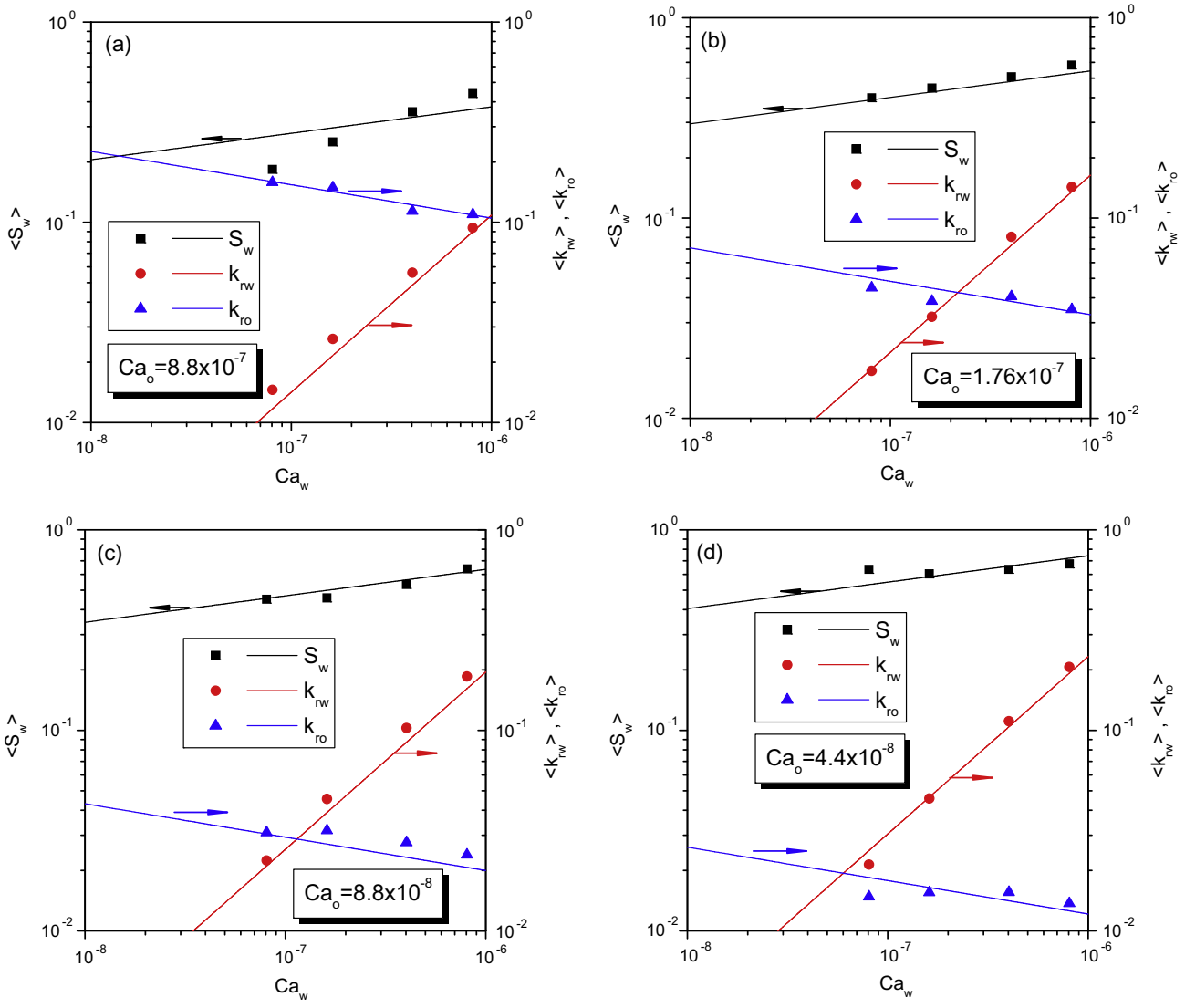

Fig. 3. Soil column-averaged water saturation and water/oil relative permeability as functions of Ca_w at various values of Ca_o.

Eqs. (4) and (5) and the results are compared with corresponding ones of 2-D porous media in Tables 3 and 4, respectively.

In the 3-D soil column, the capillary end effect induces stronger dependence of the measured relative permeability functions on boundary conditions and results in a_w, a_o values that are higher than those of the 2-D pore network (Tables 3 and 4). As the viscosity ratio, κ, decreases, there is a higher probability for the disconnection of connected oil pathways by injected water, leading to a respectable reduction of $\langle k_{ro}\rangle$ at increasing Ca_w values. This is reflected in a higher e_w value (Table 3).

The water relative permeability is more sensitive to Ca_w and less sensitive to Ca_o (Figs. 3 and 4). As Ca_w increases, water starts occupying a gradually increasing number of non-interrupting and sample-spanning clusters of the pore space thus enhancing substantially the water hydraulic conductivity or equivalently increasing the value of $\langle k_{rw}\rangle$ (Fig. 3). The viscous coupling between oil and water is reflected in the weak but negative effect of Ca_w on $\langle k_{ro}\rangle$ (Fig. 3). In general, the flow regime is a mixture of connected pathways flows (CPF) and ganglion dynamics (GD), and the decrease of $\langle k_{ro}\rangle$ at increasing Ca_w values is due to the decrease of the oil flow fraction through CPF and the subsequent increase of the oil transfer by GD.

Likewise, the oil relative permeability is more sensitive to Ca_o and less sensitive to Ca_w (Figs. 3 and 4). As Ca_o increases, a higher number of network spanning clusters are occupied by connected oil pathways leading to a substantial increase of $\langle k_{ro}\rangle$ (Fig. 4). On the other hand, $\langle k_{rw}\rangle$ becomes more sensitive to Ca_o and b_o is higher in the 3-D system (Table 4) because of the co-existence of water and oil sample-spanning clusters over a broader Ca_w range.

The above-described sensitivity of water saturation and oil/water relative permeability to water and oil capillary number can explain completely the experimentally measured relative permeability curves (Fig. 5). In the 3-D soil column tests the variation of $\langle S_w\rangle$ with Ca_w is described by the scaling law

$$Ca_w \propto \langle S_w\rangle^{1/m_w} \tag{13}$$

Therefore, the variation of $\langle k_{rw}\rangle$ and $\langle k_{ro}\rangle$ with S_w will follow the scaling laws

$$\langle k_{rw}\rangle \propto \langle S_w\rangle^{b_w/m_w} \tag{14}$$

$$\langle k_{ro}\rangle \propto \langle S_w\rangle^{e_w/m_w} \tag{15}$$

In the experiments performed in the 2-D pore network at two values of the viscosity ratio, the variation of $\langle S_w\rangle$ with Ca_o is described by the scaling law

$$Ca_o \propto \langle S_w\rangle^{1/m_o} \tag{16}$$

Therefore, the variation of $\langle k_{rw}\rangle$ and $\langle k_{ro}\rangle$ with S_w will follow the scaling laws

$$\langle k_{rw}\rangle \propto \langle S_w\rangle^{b_o/m_o} \tag{17}$$

$$\langle k_{ro}\rangle \propto \langle S_w\rangle^{e_o/m_o} \tag{18}$$

Based on the aforementioned scaling relationships, it turns out that the different slopes observed in $\langle k_{rw}\rangle(\langle S_w\rangle)$ and $\langle k_{ro}\rangle(\langle S_w\rangle)$ functions between the 3-D soil column (Fig. 5a) and the 2-D pore network (Fig. 5b and c) are consistent with the power-law dependence of relative permeabilities on Ca_o and Ca_w, respectively (Table 5). The aforementioned exponents were overestimated only for the 3-D sandpack and over the highest oil capillary number (Fig. 5a). This overestimation might be attributed to the inability of a power model, Eq. (6), with unique exponents m_o, m_w, and coefficient, a_s, to reproduce the, $\langle S_w\rangle(Ca_w)$ relation over high Ca_o values (Fig. 3a). At high Ca_o values, the flow regime is clearly dominated by continuous oil pathway flow (Avraam and Payatakes, 1995) and probably a higher value of exponent m_w should be estimated from the corresponding data for reproducing the

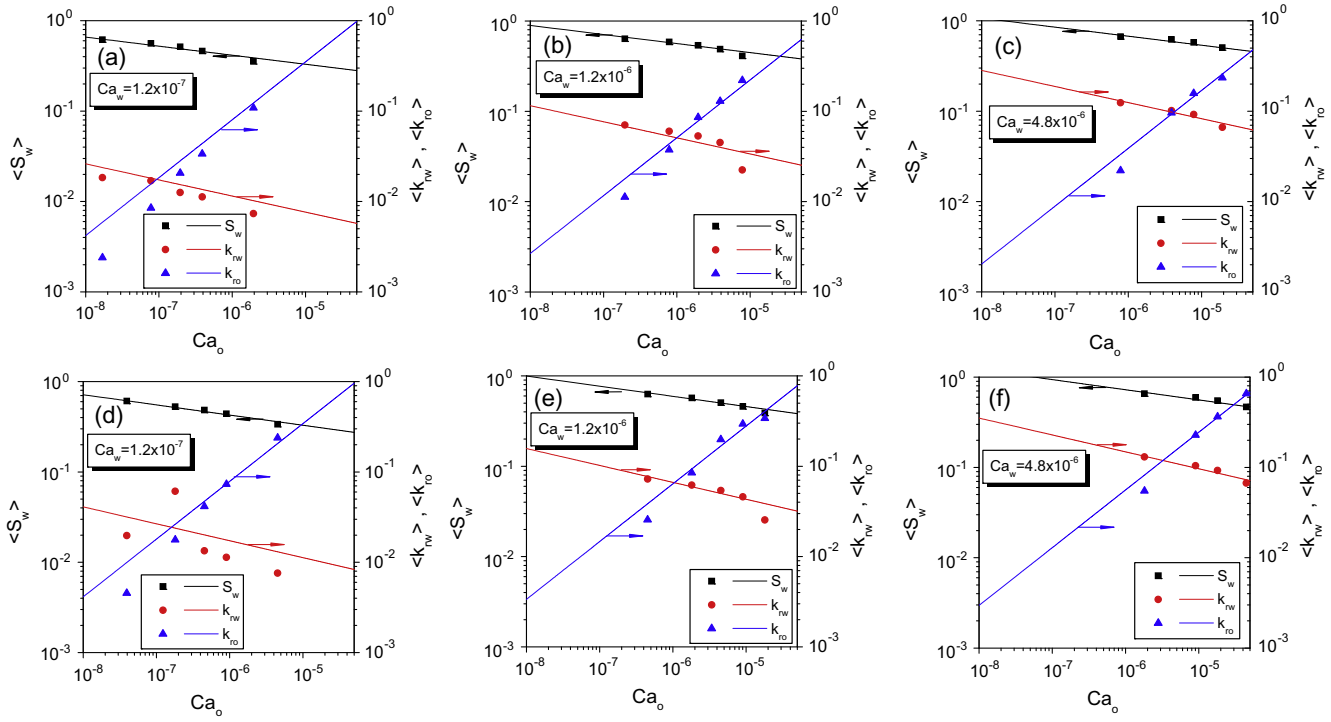

Fig. 4. 2D network-averaged water saturation and water/oil relative permeability as functions of Ca_o at various values of Ca_w for oil to water viscosity ratio (a–c) κ = 1.45, (d–f) κ = 3.35.

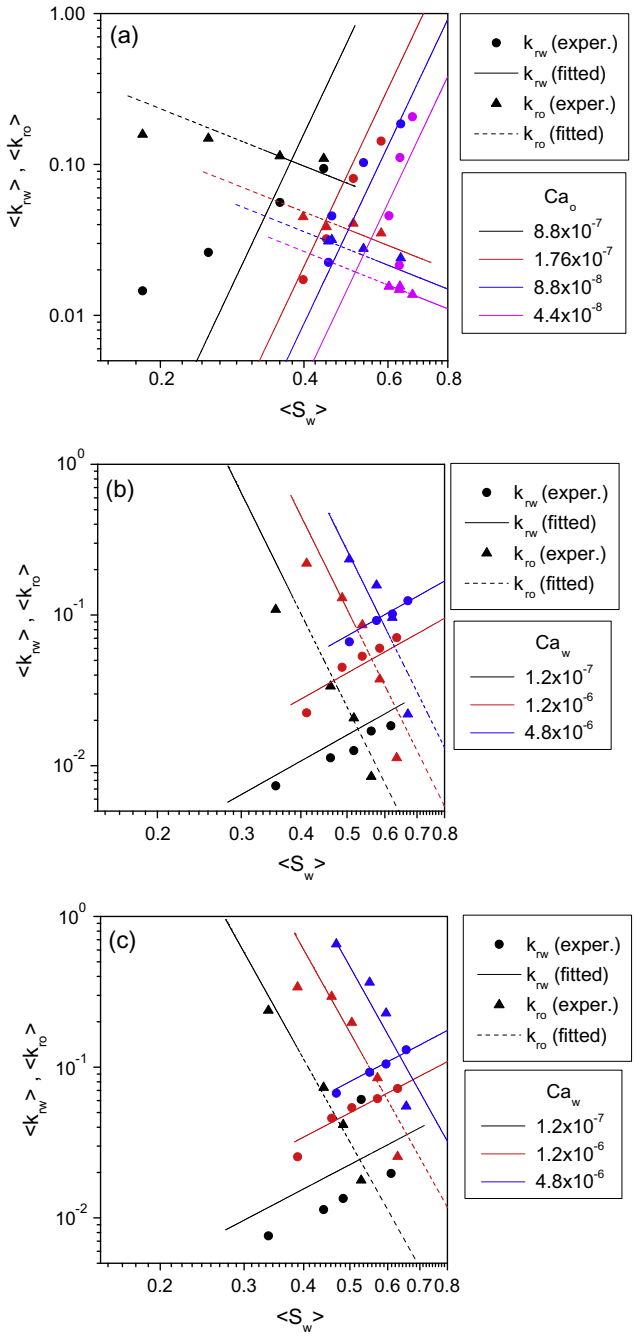

Fig. 5. Relative permeability curves for (a) 3-D soil column and $\kappa = 1.0$, (b) 2-D pore network and $\kappa = 1.45$, (c) 2-D pore network and $\kappa = 3.35$.

Table 5
Power laws correlating relative permeability with water saturation (the power laws of shaded boxes are predictions that are not shown in Fig. 5).

Power law scaling	2-D glass-etched pore network ($\kappa = 1.45$)	2-D glass-etched pore network ($\kappa = 3.35$)	3-D soil column
$k_{rw} \propto S_w^{b_w/m_w}$	$k_{rw} \propto S_w^{4.9}$	$k_{rw} \propto S_w^{4.05}$	$k_{rw} \propto S_w^{6.69}$
$k_{ro} \propto S_w^{e_w/m_w}$	$k_{ro} \propto S_w^{-1.49}$	$k_{ro} \propto S_w^{-0.63}$	$k_{ro} \propto S_w^{-1.26}$
$k_{rw} \propto S_w^{b_o/m_o}$	$k_{rw} \propto S_w^{1.78}$	$k_{rw} \propto S_w^{1.66}$	$k_{rw} \propto S_w^{1.13}$
$k_{ro} \propto S_w^{e_o/m_o}$	$k_{ro} \propto S_w^{-6.4}$	$k_{ro} \propto S_w^{-5.68}$	$k_{ro} \propto S_w^{-3.18}$

experimentally measured $\langle k_{rw}\rangle(\langle S_w\rangle)$ and $\langle k_{ro}\rangle(\langle S_w\rangle)$ with Eqs. (14) and (15) (Fig. 5a).

In general, the growth of the transient two-phase displacement front in homogeneous and water-wet porous media is governed by the interactions of viscous and capillary forces. By using scaling arguments of the gradient percolation theory at the limit of high viscosity ratio, the following approximate power laws were obtained for drainage processes (Tsakiroglou et al., 2003)

$$\langle S_o\rangle \propto Ca_o^{\beta_p/(\mu-\beta_p+\nu_p+1)} \tag{19}$$

$$\langle k_{ro}\rangle \propto \mathrm{Ca}_o^{\mu/(\mu-\beta_p+\nu_p+1)} \tag{20}$$

where $\langle S_o\rangle$ is the total oil saturation, and μ, β_p, ν_p are the universal scaling exponents for the pore system conductivity, accessibility and correlation length, respectively (Sahimi, 1995; Table 6). By regarding the flow-rate dependent imbibition as a gradient percolation process, we expect to obtain analogous power laws for the wetting phase, namely

$$\langle S_w\rangle \propto \mathrm{Ca}_w^{\beta_p/(\mu-\beta_p+\nu_p+1)} \tag{21}$$

$$\langle k_{rw}\rangle \propto \mathrm{Ca}_w^{\mu/(\mu-\beta_p+\nu_p+1)} \tag{22}$$

If we make the over-simplifying assumption that the (stationary) steady-state two-phase flow regime is generated by the superposition of the transient displacement fronts of drainage and imbibition processes, then according to Eqs. (20)–(22) and Table 6, the following power laws are obtained

$$\begin{aligned}&\langle S_w\rangle \propto Ca_w^{0.04} \text{ for a } 2-\mathrm{D} \text{ system, and}\\ &\langle S_w\rangle \propto Ca_w^{0.118} \text{ for a } 3-\mathrm{D} \text{ system}\end{aligned} \tag{23}$$

$$\begin{aligned}&\langle k_{ro}\rangle \propto Ca_o^{0.37} \text{ for a } 2-D \text{ system, and}\\ &\langle k_{ro}\rangle \propto Ca_o^{0.58} \text{ for a } 3-\mathrm{D} \text{ system}\end{aligned} \tag{24}$$

$$\begin{aligned}&\langle k_{rw}\rangle \propto Ca_w^{0.37} \text{ for a } 2-\mathrm{D} \text{ system, and}\\ &\langle k_{rw}\rangle \propto Ca_w^{0.58} \text{ for a } 3-\mathrm{D} \text{ system}\end{aligned} \tag{25}$$

The gradient percolation approach sub-estimates the m_w exponent for 2-D systems (Eq. (23), Table 2). For topological reasons, in a 2-D system, the GD is expected to become the dominant flow regime over a broader range of Ca_w and $\langle S_w\rangle$ values compared to the 3-D system. On the other hand, the gradient percolation approach is unable to account the effect of GD on water saturation, and predict the correct value of exponent m_w. Moreover, the higher e_o and b_w values for 3-D systems (Tables 3 and 4) are qualitatively consistent with the corresponding scaling exponents predicted by the gradient percolation approach, Eqs. (24) and (25). The "bi-continuity" of the 3-D systems allows the coexistence of sample-spanning percolation clusters for both fluids so that the contribution fraction of the conductivity of these clusters to the effective permeability of fluids is expected to be higher. However, the e_o and b_w values estimated by the steady-state experiments (Tables 3 and 4) are higher than those predicted by percolation approach, Eqs. (24) and (25), due to the significant contribution of the hydraulic conductivity of moving oil ganglia to the effective permeabilities (Valavanides and Payatakes, 2001, 2002).

Table 6
Universal scaling exponents.

Exponent	2-D systems	3-D systems
b_p	0.139	0.41
ν_p	1.33	0.88
μ	1.3	2.0

Conclusions

A suitable and cost-effective method of measuring the water saturation in porous media relies on the inversion of electrical resistivity data by using an Archie type power law. Attention must be paid on the accurate estimation of saturation exponent which, in general, may change substantially with various parameters (e.g. wettability, pore space morphology, fluid system properties, etc.). For a given porous medium and an oil/water system, the steady-state relative permeability may change profoundly with the water and oil capillary numbers. Two-phase flow tests in a 2-D glass-etched pore network, and a 3-D sandpack show that the water saturation along with the water and oil relative permeability may be regarded as power functions of the oil and water capillary numbers. In that context, the scaling relationships connecting each relative permeability with saturation are obtained. The exponents appearing in the power law functions vary with the dimensionality and viscosity ratio, while the pre-exponential factors depend strongly on the boundary conditions. The variation of the exponents with pore system dimensionality is in qualitative agreement with the scaling behavior predicted by the gradient percolation approach. It is worth mentioning that percolation theory is unable to account for the effect of the moving ganglia populations on the relative permeability functions, unlike pore network simulators do.

Additional research is needed toward elucidating the sensitivity of the relative permeability of wetting and non-wetting fluid to capillary number(s) over low (gas/water) and high (viscous oil/water) values of the viscosity ratio where the viscous forces of the one fluid almost vanish. Having succeeded in mapping the behavior of relative permeabilities over the parameter space, we will be able to make a decision for the dependence of local (core-scale) relative permeability of each fluid on the local flow rates and choose the most suitable constitutive equations when simulating transient problems of two-phase flow at a macroscopic scale in a reservoir. Moreover, there is a need for extrapolating the results of steady-state two-phase flow experiments to mixed-wet porous media. In this context, first the two-phase flow regimes must be reconsidered in the light of mixed-wet solid surfaces, and then, examine extensively the sensitivity of relative permeabilities to capillary numbers.

Acknowledgements

This research has been co-financed by the European Union (European Social Fund-ESF) and Greek national funds through the Operational Programme "Education and Lifelong Learning 2007–2013, action: "Archimedes III – Funding of research groups in T.E.I.".

References

Aggelopoulos, C.A., Tsakiroglou, C.D., 2008. The effect of micro-heterogeneity and capillary number on capillary pressure and relative permeability curves of soils. Geoderma 148, 25–34.

Aker, E., Måløy, K.J., Hansen, A., Batrouni, G.G., 1998. A two-dimensional network simulator for two-phase flow in porous media. Transport Porous Media 32 (2), 163–186.

Avraam, D.G., Payatakes, A.C., 1995a. Flow regimes and relative permeabilities during steady-state two-phase flow in porous media. J. Fluid Mech. 293, 207–236.

Avraam, D.G., Payatakes, A.C., 1995b. Generalized relative permeability coefficients during steady-state two-phase flow in porous media and correlation with the flow mechanisms. Transport Porous Media 20, 135–168.

Avraam, D.G., Payatakes, A.C., 1999. Flow mechanisms, relative permeabilities, and coupling effects in steady-state two-phase flow through porous media. The case of strong wettability. Ind. Eng. Chem. Res. 38, 778–786.

Avraam, D.G., Kolonis, G.B., Roumeliotis, T.C., Constantinides, G.N., Payatakes, A.C., 1994. Steady-state two-phase flow through planar and nonplanar model porous media. Transport Porous Media 16, 75–101.

Ayub, M., Bentsen, R.G., 2001. An apparatus for simultaneous measurement of relative permeability and dynamic capillary pressure. Petrol. Sci. Technol. 19, 1129–1154.

Ayub, M., Bentsen, R.G., 2004. Experimental testing of interfacial coupling in two-phase flow in porous media. Petrol. Sci. Technol. 23, 863–897.

Bentsen, R.G., Manai, A.A., 1991. Measurement of co-current and countercurrent relative permeability curves using the steady-state method. AOSTRA J. Res. 7, 169–181.

Berg, S., Ott, H., 2012. Stability of CO_2–brine immiscible displacement. Int. J. Greenhouse Gas Control 11, 188–203.

Blunt, M., King, P., 1991. Relative permeabilities from two- and three-dimensional pore-scale network modelling. Transport Porous Media 6 (4), 407–433.

Bradford, S.A., Abriola, L.M., Leij, F.J., 1997. Wettability effects on two- and three fluid relative permeabilities. J. Contam. Hydrol. 28, 171–191.

Constantinides, G.N., Payatakes, A.C., 1996. Network simulation of steady-state two-phase flow in consolidated porous media. AIChE J. 42, 369–382.

Dias, M.M., Payatakes, A.C., 1986a. Network models for two-phase flow in porous Media. Part 1: Immiscible displacement of non-wetting fluids. J. Fluid Mech. 164, 305–336.

Dias, M.M., Payatakes, A.C., 1986b. Network models for two-phase flow in porous Media. Part 2. Motion of oil ganglia. J. Fluid Mech. 164, 337–358.

Erpelding, M., Sinha, S., Tallakstad, K.T., Hansen, A., Flekkoy, E.G., Maloy, K.J., 2013. History independence of steady-state in simultaneous two-phase flow through two-dimensional porous media. Phys. Rev. E 88, 053004 (1–12).

Gao, S., Meegoda, J.N., Hu, L., 2013. Simulation of dynamic two-phase flow during multistep air sparging. Transport Porous Media 96 (1), 173–192.

Gladkikh, M., Bryant, S.L., 2006. Influence of wettability on petrophysical properties during imbibition in a random dense packing of equal spheres. J. Petrol. Sci. Eng. 52, 19–34.

Gutierez, B., Juarez, F., Ornelas, L., Zeppieri, S., Lopez de Ramos, A., 2008. Experimental study of gas–liquid two-phase flow in glass micromodels. Int. J. Thermophys. 29, 2126–2135.

Hashemi, M., Dabir, B., Sahimi, M., 1999. Dynamics of two-phase flow in porous media: simultaneous invasion of two fluids. AIChE J. 45, 1365–1382.

Huang, H., Lu, X.-Y., 2009. Relative permeabilities and coupling effects in steady-state gas-liquid flow in porous media: a lattice Boltzman study. Phys. Fluids 21, 092104 (1–10).

Jackson, M.D., Valvante, P.H., Blunt, M.J., 2003. Prediction of wettability variation and its impact on flow using pore- to reservoir-scale simulations. J. Petrol. Sci. Eng. 39, 231–246.

Joekar-Niasar, V., Hassanizadeh, S.M., Leijnse, A., 2008. Insights into the relationships among capillary pressure, saturation, interfacial area and relative permeability using pore-network modeling. Transport Porous Media 74, 201–219.

Knudsen, H.A., Hansen, A., 2002. Relation between pressure and fractional flow in two-phase flow in porous media. Phys. Rev. E 65 (5), 056310 (1–10).

Kuttanikkad, S.P., Orat, M., Pauchet, J., 2011. Pore-network simulations of two-phase flow in a thin porous layer of mixed wettability: application to water transport in gas diffusion layers of proton exchange membrane fuel cells. J. Power Sources 196, 1145–1155.

Lackner, A.S., Torsaeter, O., 2006. Effects of pressure and wettability on residual phase saturation in sandstone rock. J. Petrol. Sci. Eng. 52, 237–243.

Landry, C.J., Karpyn, Z.T., Ayala, O., 2014. Relative permeability of homogeneous-wet and mixed-wet porous media as determined by pore-scale lattice Boltzmann modeling. Water Resour. Res. 50, 3672–3689.

Lenormand, R., Zarcone, C., Sarr, A., 1983. Mechanisms of the displacement of one fluid by another in a network of capillary ducts. J. Fluid Mech. 135, 337–353.

Lenormand, R., Touboul, E., Zarcone, C., 1988. Numerical models and experiments on immiscible displacement in porous media. J. Fluid Mech. 189, 165–187.

Li, H., Pan, C., Miller, C.T., 2005. Pore-scale investigation of viscous coupling effects for two-phase flow in porous media. Phys. Rev. E 72, 026705 (1–12).

Payatakes, A.C., 1982. Dynamics of oil ganglia during immiscible displacement in water-wet porous media. Ann. Rev. Fluid Mech. 14, 365–393.

Ramstad, T., Hansen, A.H., 2006. Cluster evolution in steady-state two-phase flow in porous media. Phys. Rev. E 73, 026306 (1–11).

Ramstad, T., Idowu, N., Nardi, C., Oren, P.-E., 2012. Relative permeability calculations from two-phase flow simulations directly on digital images of porous rocks. Transport Porous Media 94, 487–504.

Raoof, A., Hassanizadeh, S.M., 2012. A new formulation for pore-network modeling of two-phase flow. Water Resour. Res. 48 (1), W01514.

Sahimi, M., 1995. Flow and Transport in Porous Media and Fractured Rock: From Classical Methods to Modern Approaches. VCH Weinheim, Germany.

Sinha, S., Hansen, A., 2012. Effective rheology of immiscible two-phase flow in porous media. Europhys. Lett. 99, 44004 (1–6).

Stewart, W.E., Caracotsios, M., 2008. Computer-aided modeling of reactive systems. Wiley-Interscience, Hoboken, NJ, USA.

Tallakstad, K.T., Lovoll, G., Knudsen, H.A., Ramstad, T., Flekkoy, E.G., Maloy, K.J., 2009a. Steady-state, simultaneous two-phase flow in porous media: an experimental study. Phys. Rev. E 80, 036308 (1–13).

Tallakstad, K.T., Knudsen, H.A., Ramstad, T., Lovoll, G., Maloy, K.J., Toussaint, R., Flekkoy, E.G., 2009b. Steady-state two-phase flow in porous media: statistics and transport properties. Phys. Rev. Lett. 102, 074502 (1–4).

Theodoropoulou, M.A., Sygouni, V., Karoutsos, V., Tsakiroglou, C.D., 2005. Relative permeability and capillary pressure functions of porous media as related to the displacement growth pattern. Int. J. Multiph. Flow 31, 1155–1180.

Tsakiroglou, C.D., 2014. Computation of the two-phase flow properties of intermediate-wet porous media: a pore network approach. Can. J. Chem. Eng. 92, 515–523.

Tsakiroglou, C.D., Fleury, M., 1999. Resistivity index of fractional wettability porous media. J. Petrol. Sci. Eng. 22, 253–274.

Tsakiroglou, C.D., Theodoropoulou, M., Karoutsos, V., 2003. Non-equilibrium capillary pressure and relative permeability curves of porous media. AIChE J. 49, 2472–2486.

Tsakiroglou, C.D., Avraam, D.G., Payatakes, A.C., 2007. Transient and steady-state relative permeabilities from two-phase flow experiments in planar pore networks. Adv. Water Res. 30, 1981–1992.

Valavanides, M.S., Payatakes, A.C., 2001. True-to-mechanism model of steady-state two-phase flow in porous media, using decomposition into prototype flows. Adv. Water Resour. 24, 385–407.

Valavanides, M.S., Payatakes, A.C., 2002. Effects of Pore Network Characteristics on Steady-State Two-Phase Flow Based on a True-to-Mechanism Model (DeProF). SPE-78516, Paper Presented at 10th Abu Dhabi International Petroleum Exhibition and Conference (ADIPEC), pp. 379–387.

Valavanides, M.S., Constantinides, G.N., Payatakes, A.C., 1998. Mechanistic model of steady-state two-phase flow in porous media based on ganglion dynamics. Transport Porous Media 30, 267–299.

Valvatne, P.H., Blunt, M.J., 2004. Predictive pore-scale modeling of two-phase flow in mixed wet media. Water Resour. Res. 40 (7), W07406 (1–21).

Vizika, O., Avraam, D.G., Payatakes, A.C., 1994. On the role of the viscosity ratio during low-capillary number forced imbibition in porous media. J. Colloid Int. Sci. 165, 386–401.

Wang, X., Van Nguyen, T., Hussey, D.S., Jacobson, D.L., 2010. An experimental study of relative permeability of porous media used in proton exchange membrane fuel cells. J. Electrochem. Soc. 157 (12), B1777–B1782.

Xu, B., Yortsos, Y.C., Salin, D., 1998. Invasion percolation with viscous forces. Phys. Rev. E 57, 739–751.

Yiotis, A.G., Talon, L., Salin, D., 2013. Blob population dynamics during immiscible two-phase flows in reconstructed porous media. Phys. Rev. E 87, 033001 (1–12).